Commun Transp Res

Research Article

Leveraging distributed acoustic sensing for large-scale expressway traffic state perception

Yang Ma[1], Dianwei Zhou[1], Yang Liu[2], Yu Kang[3,4,✉], Wenjun Lv[4,5], Said M. Easa[6], Yiik Diew Wong[7]

Cite this article: https://doi.org/10.26599/COMMTR.2026.9640043

ABSTRACT: This paper introduces distributed acoustic sensing (DAS) as an emerging sensing technique for large-scale traffic state perception (TSP) on expressways. By enabling optical fibers to operate as dense sensing arrays, DAS offers a promising solution for continuous traffic monitoring along expressway corridors. However, the raw traffic information extracted from DAS is inaccurate, which limits its direct application to large-scale TSP. This study proposes a physics-informed neural network (PINN) framework for DAS-based TSP. A physics-based DAS simulation platform is developed and validated against field observations which provides a flexible testbed for generating data under diverse traffic scenarios. On this basis, two network architectures, ResUNet and Fourier Neural Operator, are investigated in combination with three types of traffic flow constraints, namely the Lighthill-Whitham-Richards (LWR) model, LWR with a fundamental diagram, and the Aw-Rascle-Zhang model. Totally, 16 PINN models are constructed and evaluated. The results show that the proposed PINN framework effectively improves the accuracy of DAS-based TSP compared to the solely data-driven baselines. Among the physical constraints considered, the LWR-based models show the best overall performance. In addition, few-shot transfer learning can enhance model performance in previously unseen scenarios, demonstrating the potential of the proposed framework for adaptation to site-specific deployment conditions.

KEYWORDS: large-scale traffic state perception, physics-informed deep learning, distributed acoustic sensing, ubiquitous traffic sensing

1 Introduction

1.1. Background

Large-scale and real-time traffic state perception (TSP) on expressways is fundamental to various applications within intelligent transportation systems, including proactive traffic management, incident detection, etc. (An et al., 2025; Ma et al., 2025). However, existing sensing technologies for TSP, such as inductive loops, cameras, and radar, have inherent limitations, as illustrated in Fig. 1. Specifically, these conventional methods typically offer point-based or narrow-range measurements, and require substantial installation and maintenance costs (Narri et al., 2025). Their performance may also degrade substantially under adverse weather conditions, including fog, rain, and snow (Klein, 2024). In addition, high-resolution imaging systems may raise privacy concerns. Although camera-radar fusion systems can improve sensing capability, their deployment remains challenging because of high costs and complex calibration requirements in heterogeneous environments (Tu et al., 2024; Wang et al., 2025), rendering them impractical for scalable, end-to-end TSP across hundreds of kilometers of expressway corridor.

Distributed acoustic sensing (DAS), an emerging fiber optic sensing technology, has shown significant potential for traffic monitoring (An et al., 2023; Urquijo et al., 2023). Based on the principle of Rayleigh backscattering, DAS transforms standard fiber optic cables into spatially continuous arrays of vibration sensors, enabling real-time acoustic signal monitoring by capturing subtle subsurface deformations induced by vehicles along the fiber. As such, DAS can collect vibration signals over long distances (e.g., 20 km) with meter-level spatial resolution and sub-millisecond temporal precision. In this regard, compared to traditional sensors as illustrated in Fig. 1, DAS offers both extended sensing range and high spatiotemporal resolution (Fakhruzi et al., 2025; He and Liu, 2021).

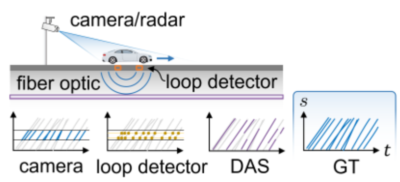

Fig. 1. Illustration of data characteristics of different sensing technologies.

Unlike traditional sensors that require installation, DAS can leverage existing fiber optic infrastructure, and thereby eliminate the need for procurement and deployments of new hardware. DAS' immunity to electromagnetic interference, all-weather operational capability, and maintenance-free nature make it well-suited for large-scale and long-term infrastructure monitoring of linear assets such as railways, bridges, tunnels, and pipelines (Z. Chen et al., 2024; Kishida et al., 2024; Lienhart et al., 2023; Rahman et al., 2024; Rossi et al., 2022; Zhou and Wu, 2024).

Although fiber optic-based traffic sensing is not a novel concept, previous implementations primarily relied on discrete and specialized Fiber Bragg Grating (FBG) sensors embedded at specific locations, such as toll booths or bridges (Yuan et al., 2020; Zhang et al., 2022; Zhu et al., 2022). FBG systems, illustrated in Fig. 2, can provide high precision for localized strain or temperature measurements (Wang et al., 2020).

[1]School of Automotive and Transportation Engineering, Hefei University of Technology, Hefei 230009, China. [2]School of Vehicle and Mobility, Tsinghua University, Beijing 100084, China. [3]School of Electrical Engineering and Automation, Hefei University of Technology, Hefei 230009, China. [4]Department of Automation, University of Science and Technology of China, Hefei 230026, China. [5]Institute of Advanced Technology, University of Science and Technology of China, Hefei 230088, China. [6]Department of Civil Engineering, Toronto Metropolitan University, Toronto ON M5B 2K3, Canada. [7]School of Civil and Environmental Engineering, Nanyang Technological University, Singapore 639798, Singapore.

✉ Corresponding author. E-mail: kangduyu@hfut.edu.cn

Received: April 10, 2026; Revised: May 28, 2026; Accepted: August 3, 2026

However, FBG sensors are inherently sparse, typically deployed at intervals greater than 100 meters, and may require specialized installation, active interrogation units, and individual calibration.

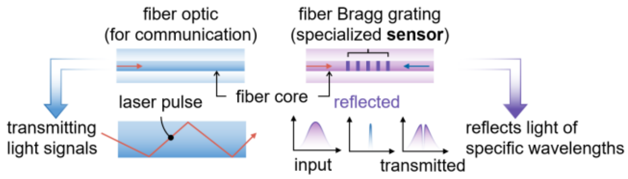

Fig. 2. Fiber optic vs FBG.

In contrast, this study aims to utilize existing telecommunication fibers already buried alongside most expressways. By employing DAS interrogators, these fibers can operate passively without interrupting communication services (Narisetty et al., 2021). In this regard, DAS may represent a paradigm shift, if well developed, from capital-intensive, customized sensor networks to infrastructure-as-sensor solutions without deployment of new facilities.

1.2. Problem context

Although DAS is a promising technique to achieve large-scale and ubiquitous TSP on expressways, the nature of DAS data presents several new challenges. The raw measurements of DAS are inherently noisy and indirect. As illustrated in Fig. 1, although existing DAS-based perception methods can use deep learning to delineate vehicle trajectory-like patterns from the signal matrix (Thomas et al., 2024; W. Zhang et al., 2025), the precision in terms of DAS-captured vehicle parameters can be lower compared to a dedicated point sensor like a calibrated inductive loop or a high-resolution camera. More specifically, the signal becomes highly ambiguous when multiple vehicles travel alongside in parallel. In such cases, vibration signatures may overlap and mix, making parallelly driving vehicles difficult to be distinguished (Ouellet et al., 2024). This interference may further lead to frequent trajectory miss-detections, where parts of the vehicle traces are fragmented or completely absent. As a result, the accuracy of traffic state sensing derived from DAS remains insufficient, and the reconstructed spatiotemporal traffic state diagrams (e.g., flow and speed maps) are typically coarse and lack fine-grained dynamic details.

1.3. Objective and contributions

To address this gap, the main objective of this study is to investigate the feasibility of applying physics-informed deep learning (PIDL) to enable DAS-based large-scale TSP on expressways. Because DAS generates continuous yet inherently coarse spatiotemporal traffic state maps (STM), we formulate the DAS-based TSP task as an image restoration problem in this study.

The specific contributions of this study are threefold as follows:

a) We develop a physics-based DAS simulation framework to evaluate the performance of different TSP models under controlled yet realistic conditions;

b) We construct a set of PINN models, each integrating a different combination of deep neural network (DNN) architectures and traffic flow constraints, for STM restoration, and we qualitatively and quantitatively compare different models' accuracy performance;

c) We examine whether the trained DNN can be effectively applied to new scenarios through small-sample transfer learning.

2 Literature review

2.1. DAS applications

Existing studies utilizing DAS for engineering applications can be generally divided into large-scale and small-scale categories. Owing to DAS' capability of capturing continuous and large-scale vibration signals, it has been extensively applied in geophysics, disaster monitoring (e.g., avalanches, landslides, rockfalls), perimeter security, etc. (Han et al., 2024; Hubbard et al., 2022; Xie et al., 2023).

Some studies have also tried to apply DAS technologies in urban traffic monitoring. For instance, researchers used the deployed urban fiber optic cables for city-wide vehicle tracking, stop-and-go wave analysis, and intersection traffic flow estimation (Y. Chen et al., 2024; Li et al., 2026; Liu et al., 2025; Song et al., 2026). A trial analysis in the city of Granada further demonstrated the potential of DAS as an effective tool for urban traffic monitoring (Fakhruzi et al., 2025). These applications illustrate DAS's capability for large-scale traffic characterization without line-of-sight restrictions. However, existing studies using DAS for large-scale traffic monitoring or analysis focus on capturing the general trends of traffic dynamic patterns, rather than performing accurate and continuous traffic state estimation.

At a smaller scale, DAS has shown encouraging performance in more detailed traffic sensing tasks. Canudo et al. (2024) used chirped-pulse DAS technology within intelligent traffic monitoring systems to acquire individual vehicle and road state information by monitoring vehicle-induced vibrations. Zhang et al. (2025) leveraged DAS data to recognize vehicle spatiotemporal trajectories through deep learning techniques. Some studies also proposed to combine DAS data with visual information and thus achieved high-accuracy detection and classification performance for vehicle detection and speed estimation through deep learning frameworks (Cohen et al., 2025; Khacef et al., 2025; Tomasov et al., 2025). These developments demonstrate the potential of DAS in collecting detailed traffic data. However, the approaches for accurate traffic state estimation were all based on a small scale. There is a research gap regarding the application for continuous and precise TSP on large-scale expressways.

2.2. Large-scale Traffic State Estimation on Expressways

Over the past decades, TSP on long-distance expressways has evolved through several methodological phases, encompassing theoretical models, machine learning (ML), deep learning (DL), and the emerging PIDL approach, as summarized in Tab. 1.

Early approaches for TSP relied on classical traffic flow theory, such as the Lighthill-Whitham-Richards (LWR) model and the Greenshields model (Wang and Papageorgiou, 2005). These models describe the macroscopic characteristics of traffic flow, including density, speed, and flow rate, using partial differential equations (Agrawal et al., 2023). The fundamental process involves discretizing road networks into segments and applying conservation laws to estimate traffic states based on observed boundary conditions. Data sources for these models traditionally included inductive loops, which provide point measurements of vehicle count and speed, and later, radar systems (Seo et al., 2017). While these methods offer a foundational understanding of traffic dynamics and are computationally efficient, their simplified assumptions on driver behaviors and road geometry may fail themselves to capture complex, non-linear traffic phenomena (Zhang et al., 2023).

With the increasing availability of diverse traffic data sources, ML techniques gradually became an important alternative for TSP. These methods include support vector machines, K-nearest neighbors, random forests, etc. (Darwish et al., 2024). The basic process of ML involves training a model on historical traffic data (e.g., speed, volume, occupancy from inductive loops, cameras, or ETC systems) to learn non-linear relationships and infer current traffic conditions in unobserved areas. ML models offer improved accuracy over theoretical models by capturing intricate patterns in data without explicit physical modeling (Zhang et al., 2023). They can handle high-dimensional data (Almukhalfi et al., 2024). However, their performance heavily relies on the quality and quantity of training data, often requiring extensive feature engineering (Z. Zhang et al., 2025). Relevant data sources include camera/radar, magnetic loops, and ETC data (Guarda et al., 2024; Li et al., 2023; Liu et al., 2024).

Table 1. Summary of TSP approaches

Type	Data	Pros and cons	Representative Reference
Theoretical model	Traffic flow model parameters	Pros: efficiency and explainability Cons: challenging to model complex, non-linear traffic phenomena	(Wang et al., 2009; Wang and Papageorgiou, 2005)
ML	Camera, radar, inductive loop, and electronic toll collection (ETC)	Pros: be able to learn complex and non-linear relationships Cons: limited generalization ability, require extensive feature engineering	(Antoniou et al., 2013; Khan et al., 2017)
DNN	Camera, radar, inductive loop, and ETC, DAS	Pros: extract hierarchical features from raw traffic data Cons: require large volume of labeled data, unsatisfactory interpretability	(Bi et al., 2022; Xu et al., 2020)
PIDL	Camera, radar, inductive loop, and ETC	Pros: learn physically consistent traffic dynamics, improved generalization Cons: the formulation of physics-informed constraints can be complex	(Huang and Agarwal, 2020; J. Zhang et al., 2024)

The advent of DNN has revolutionized TSP, particularly with the development of diverse DNN architectures (Gao et al., 2024; Xia et al., 2024). These models can extract hierarchical features from raw traffic data and reduce the need for empirical feature engineering (Di et al., 2023). The DNN-based TSP typically involves feeding large datasets (e.g., from cameras, radar, or loops) into deep architectures to learn highly abstract representations. DNNs have demonstrated superior performance in capturing complex spatiotemporal dependencies and achieving high accuracy in various TSP tasks (Z. Zhang et al., 2025). They are particularly effective with large-scale datasets and can adapt to varying traffic patterns (Gao et al., 2024). However, DNNs require large volume of labeled data, and their interpretability remains a challenge (Almukhalfi et al., 2024). Data sources mainly include high-resolution data from cameras, radar, and comprehensive loop detector networks (Khacef et al., 2025).

PIDL represents a paradigm that integrates domain-specific physical laws or mathematical models directly into the deep learning framework (Huang and Agarwal, 2023; Wang et al., 2026). Recently, PIDL has gained increasing interest among researchers in this area (Di et al., 2023). Specifically, PIDL aims to leverage the strengths of both physics-based models and data-driven DNN. For TSP, PIDL models can incorporate traffic flow equations as soft or hard constraints within the neural network's loss function or architecture (Abewickrema et al., 2026; Huang and Agarwal, 2022; Rempe et al., 2021; K. Zhang et al., 2024; S. Zhang et al. 2024). This ensures that the learned traffic dynamics are physically consistent, even when data is sparse or noisy (Shi et al., 2021). The basic process of PIDL involves defining a neural network that uses traffic flow models to guide the network's training. PIDL offers improved generalization, reduced data requirements compared to purely data-driven DL, and enhanced interpretability as the predictions are grounded in physical laws (Di et al., 2023). However, the formulation of physics-informed constraints can be complex, and how to balance between data fidelity and physical adherence is an ongoing research challenge (Huang and Agarwal, 2023). This method is particularly relevant for scenarios where obtaining comprehensive, high-quality data is difficult (Luo et al., 2024).

Existing methodological paradigms for TSP, developed for localized data, are not directly transferable to DAS-based TSP on expressways. The existing method infer global traffic states from sparse and localized sensor inputs (e.g., inductive loops, point radar, cameras) (He et al., 2024; Nie et al., 2023; Seo et al., 2017; Zhao et al., 2024). This inference often relies on interpolation, extrapolation, or complex aggregation techniques to bridge data gaps, leading to potential inaccuracies in capturing the continuous and dynamic nature of highway traffic (Li et al., 2023; Liu et al., 2024; Trinh et al., 2024). DAS, in contrast, inherently provides global and continuous traffic state data along the entire fiber length, acting as a massive and distributed array of virtual sensors (Deng et al., 2025; Khacef et al., 2025; Thomas et al., 2024). This continuous spatiotemporal coverage offers an unprecedented level of detail regarding vehicle movements across long distances, overcoming the 'missing data' problem prevalent in traditional systems.

Therefore, existing TSP methodologies are not directly transferable to DAS-based TSP. A new methodological paradigm that accounts for the DAS data characteristics is needed to achieve precise DAS-based TSP.

3 Method

3.1. Overview

The proposed workflow comprises three main steps, as illustrated in Fig. 3. First, we develop a physics-based DAS simulation procedure to create large-scale spatiotemporal traffic maps and DAS signals for subsequent model training and testing. Second, we consider different combinations of DNN architectures and physical constraints in constructing PINN models. Third, we train different PINN models on the same dataset and examine their feasibility for addressing DAS-based large-scale TSP. Each part is described in detail next.

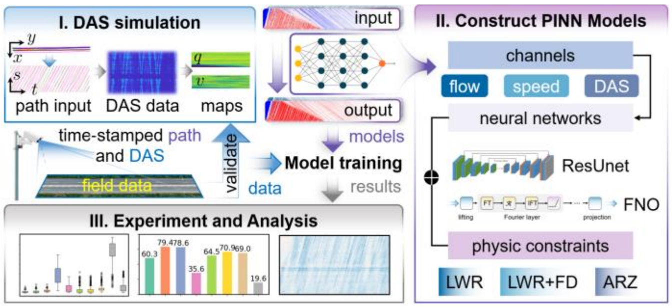

Fig. 3. Overview of the workflow.

3.2. *DAS simulation*

Due to the lack of high-quality datasets that contain both traffic flow data and DAS signals for large-scale expressways, we develop a DAS simulation framework to serve as a flexible testbed for subsequent PINN models, as shown in Fig. 4. As noted, the proposed procedure uses 2D trajectory data as input and output STM and corresponding DAS maps.

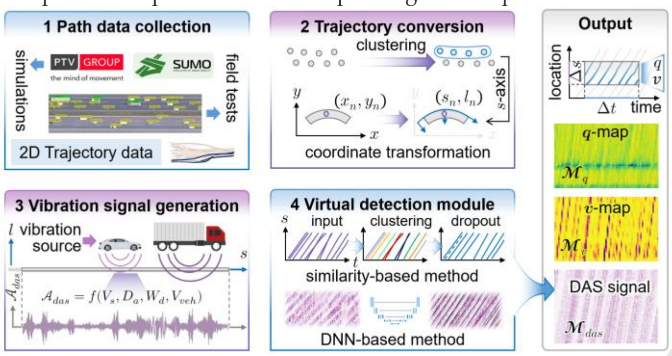

Fig. 4. General process of DAS simulation.

3.2.1 Trajectory collection and conversion

The DAS simulation procedure accepts both simulated and field collected trajectory data as input. To support the subsequent vibration signal generation, vehicle class labels shall be provided as well for the trajectories.

Since DAS vibration signals are dependent on both the lateral distance from the vehicle to the DAS optical cable and the longitudinal distance along the sensing direction, a coordinate transformation is required. Raw trajectory data typically consists of scattered spatial points in a global Cartesian coordinate system (x_n, y_n). To address this, we develop a semi-automatic trajectory conversion method to map these points into a road-aligned Frenet coordinate system.

As shown in Fig. 5, the conversion framework consists of two sequential steps: (a) a line-based growing method, and (b) spline fitting and discretization. The main purpose of the line-based growing is to extract the continuous geometric alignment of the road from scattered trajectory points. First, an empty set $\mathcal{L}$ is initialized. After manually specifying the starting point of the trajectory, the line-based growing method uses the directional vector formed by the previous point p_{n-1} and the current point p_n as a reference to construct a forward search sector, defined by a search radius r_s and an angle α_s. For the initial point, the reference direction shall be specified manually. Within this search domain, the algorithm evaluates all candidate points by calculating their deflection angles relative to the vector $\overrightarrow{p_{n-1}p_n}$. The candidate point yielding the minimum angle is selected as the new current point p_{n+1}, which is appended to the set $\mathcal{L}$, and the search window advances. This iterative process continues until no candidate points are identified within the local search domain. In this way, we can effectively delineate the continuous innermost trajectory line, as illustrated in Fig. 5(a).

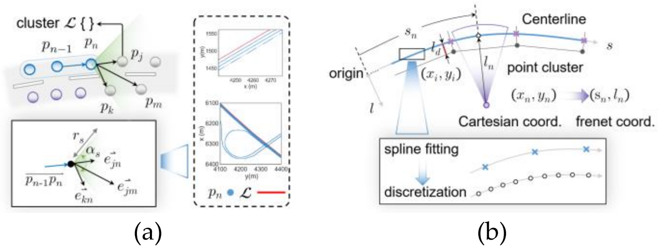

Fig. 5. Trajectory conversion. (a) line-based growing method; (b) spline fitting and discretization.

As the innermost trajectory is extracted, a cubic spline curve is applied to smoothly fit the point set $\mathcal{L}$. To ensure spatial uniformity, the fitted curve is further resampled into evenly spaced and discrete points with a uniform interval of d_s. Let l_d denote the lateral offset distance from the innermost trajectory line to the road centerline, and let β_i represent the azimuth (heading) angle at any resampled point (x_i, y_i). Based on Cartesian trigonometric relationships given by Eq. (1), the spatial coordinates of the corresponding points on the road centerline can be derived.

$$\begin{cases} x_i^c = x_i - l_d \cdot \cos\beta_i \\ y_i^c = y_i + l_d \cdot \sin\beta_i \end{cases} \tag{1}$$

where (x_i^c, y_i^c) is the road axis point corresponding to (x_i, y_i).

Based on the constructed centerline, the longitudinal coordinate s_n is calculated via cumulative distance summation along the centerline curve. To simplify the calculating process of l_n, a neighborhood search algorithm is employed for any raw trajectory point to identify its nearest corresponding point on the centerline. The Euclidean distance between the raw trajectory point and its matched centerline point defines its lateral coordinate l_n. Through this workflow, the raw trajectory points are transformed from the global Cartesian coordinate system (x_n, y_n) into the Frenet coordinate system (s_n, l_n), thus fulfilling the geometric prerequisites for accurate DAS signal simulation.

3.2.2 DAS signal generation

DAS signals could be an important data source for constructing PINN models. Therefore, based on the working mechanism of DAS, we reconstruct the mechano-optical response of a fiber-optic cable buried along an expressway, and map microscopic vehicle kinematics to optoelectronic signal matrices. The simulation process comprises three main stages, namely system configuration, vibration source modeling, and signal propagation with noise injection, as shown in Fig. 6.

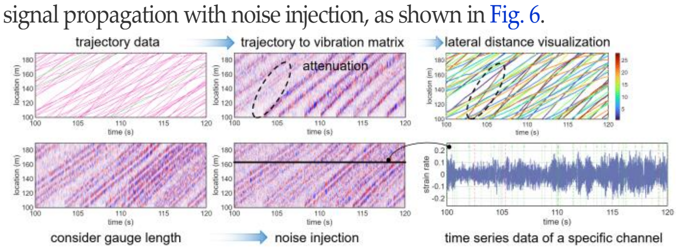

Fig. 6. Process of signal generation.

(a) Data acquisition mechanism and system configuration

The simulation emulates a phase-sensitive optical time-domain reflectometry system deployed along an expressway segment. The sensing unit interrogates a fiber optic cable of length L_e. As illustrated in Fig.7, The system's spatial resolution is governed by the gauge length L_g, while the readout channels are discretized at a spacing of Δx to guarantee Nyquist spatial sampling. The system operates at a sampling rate of f_s to capture the characteristic frequency bands (typically ranging from 5 to100 Hz) of vehicle-induced ground vibrations. The sensing geometry assumes a linear fiber deployment parallel to the road alignment, with a vertical offset distance d_{ver} from the road surface.

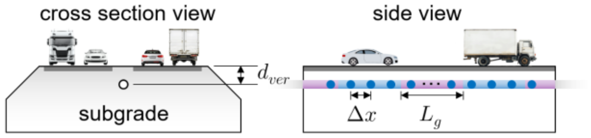

Fig. 7. Illustration of DAS parameters.

(b) Vibration source modeling

The core part of the simulation is the generation of vibration signals induced by moving vehicles. In this case, each vehicle i is treated as a moving vibration source characterized by its type C_i (e.g., passenger car, truck, bus). The spectral signature of a vehicle is represented as a weighted sum of sinusoidal components, representing the mechanical vibrations of the engine and tire-road interactions. In addition, the Doppler effect is incorporated to account for the frequency shift caused by the vehicle's velocity $v_i(t)$ relative to the sensing channel position x_{ch}. Therefore, the base vibration signal S_{src} for a vehicle is expressed as Eq. (2).

$$S_{src}(t) = A_{base} \sum_{k=1}^{K} \omega_k \sin\left(2\pi f_k \left[1 + \frac{v_i(t)}{c_{ground}} sgn\big(x_{ch} - x_i(t)\big)\right] t + \varepsilon_k\right) \tag{2}$$

where A_{base} is the amplitude scaling factor determined by vehicle mass, f_k and ω_k are the characteristic frequencies and their weights defined in the vehicle profile, c_{ground} is the ground wave velocity (set to 250 m/s in this study), $sgn(>0) = 1$ and $sgn(<0) = -1$, and ε_k is a random phase term.

(c) Signal propagation with noise injection

The transfer function from the vehicle source to the optical fiber involves geometric attenuation, medium absorption, and spatial coupling. For a vehicle axle located at x_{axle} and a sensing channel at x_{ch}, the Euclidean distance $d(t)$ is calculated considering both longitudinal and lateral separation. The attenuation function $\mathcal{A}(d)$ is modeled as Eq. (3).

$$\mathcal{A}(d) = \frac{1}{d^{\gamma}} \cdot e^{-\delta \cdot d} \tag{3}$$

where $\gamma = 2.0$ represents the geometric spreading factor for a point source in a semi-infinite medium, and $\delta = 0.005\ m^{-1}$ is the absorption coefficient.

As illustrated in Fig. 6, the vibration signal is sensitive to the distance between the vibration source and the optical fiber. Fig. 6 visualizes the lateral distance of vehicles from the fiber. It can be observed that the trajectories marked within the dashed ellipse correspond to the vehicles traveling at relatively high speeds. However, because these vehicles are located farther away from the fiber, the corresponding DAS signals exhibit noticeable attenuation. This phenomenon is consistent with the physical characteristics observed in real-world DAS measurements.

To simulate the finite spatial resolution of the DAS system, the point-source response is convolved with a spatial Gaussian kernel defined by the gauge length. The cumulative response at channel x and time t is the superposition of contributions from all axles of all active vehicles as follows:

$$\Psi(x,t) = \eta_c \sum_{i=1}^{N_{veh}} \sum_{j=1}^{N_{ax}} S_{src,i}(t) \cdot \mathcal{A}(d_{ij}) \cdot \exp\left(-\frac{(x - x_{ij})^2}{2\sigma_g^2}\right) \cdot (1 + \kappa v_i(t)) \tag{4}$$

where η_c denotes the coupling efficiency, σ_g is related to the gauge length L_g, and the term $(1 + \kappa v_i(t))$ introduces a velocity-dependent amplitude enhancement, reflecting the physical reality that faster vehicles generate higher impact energy. N_{veh} is the number of vehicles, N_{ax} denotes the number of vehicle i's axles, and x_{ij} is the longitudinal positions of the j-th axle of the i-th vehicle.

To bridge the gap between simulation and real-world conditions, a noise model $\mathcal{N}(x,t)$ is superimposed on the deterministic signal $\Psi(x,t)$. The noise component comprises three parts: a) multiplicative noise simulating the coherent fading phenomena inherent to Rayleigh backscattering, b) low-frequency spatial-correlated noise simulating background seismic activity, and c) instrument noise simulating quantization and digitization errors.

The final simulated DAS raw matrix is given by $D(x,t) = \Psi(x,t) + \mathcal{N}(x,t)$. This matrix is subsequently filtered using a bandpass filter (1 to 400 Hz) to isolate vehicle-induced signatures. Note that the final dynamic strain rate data can be used as input for the PINN models.

3.2.3 Virtual detection

The virtual detection module in the proposed DAS simulation procedure aims to generate controlled yet realistic DAS-based trajectory recognition results. In this way, DAS-captured traffic flow and speed maps can be obtained as needed with flexibility for various traffic scenarios. We consider two different ways of virtual detection in this study.

Based on empirical observations of DAS perception results, we identify three limitations of the DAS-extracted vehicle trajectories: (a) increased failure probability in distinguishing highly overlapping trajectories typically occurring during slow overtaking maneuvers, (b) random signal dropout leading to miss detections, and (c) random spatial-temporal disconnections within a single continuous trajectory. To emulate these physical and algorithmic limitations, we develop a multi-step virtual detection framework, as illustrated in Fig. 8.

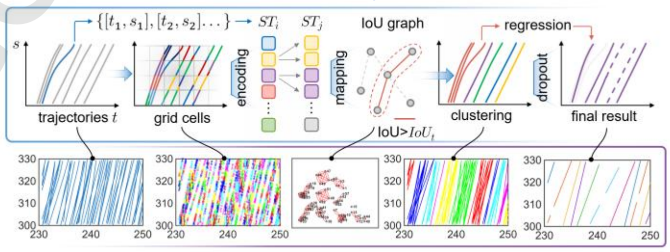

Fig. 8. Similarity-based virtual detection.

Specifically, within the distance-time spatiotemporal coordinate system, the trajectory map is uniformly partitioned into grids with dimensions of δ_s and δ_t. If multiple trajectory points fall inside the same grid cell, it indicates the corresponding trajectories overlap at that location. To guarantee computational efficiency, the center coordinates (s_g, t_g) of the grid cell are used to represent all trajectory points therein. Subsequently, a coprime product encoding function given by Eq. (5) is applied to project the 2D grid coordinates (s_g, t_g) into a unique one-dimensional (1D) code denoted as ζ. Note that the coprime product encoding function maps multi-dimensional coordinates to a unique scalar value by multiplying each dimension with a distinct prime number (Hanson, 1972). Through Eq. (5), any continuous spatiotemporal trajectory i is transformed into a discrete 1D array representation as $ST_i = \{\zeta_1, \zeta_2, \ldots, \zeta_n\}$.

$$\zeta = c_1 \cdot s_g + c_2 \cdot t_g \tag{5}$$

where c_1 and c_2 are two coprime numbers.

Building upon the 1D representation, we construct an intersection over union (IoU)-based graph to quantify trajectory similarity. In this graph, each node represents an individual spatiotemporal trajectory, and the edges denote the IoU values between pairs of trajectories. The IoU metric is calculated as twice the number of identical ζ values shared between two 1D arrays, divided by the sum of the lengths of both arrays. Based on a predefined threshold IoU_t, the algorithm clusters the originally fragmented or overlapping spatiotemporal trajectories into one group.

Following the clustering phase, a linear fitting procedure is applied to the aggregated spatiotemporal points to emulate the DAS-captured trajectory. To replicate the aforementioned signal imperfections of real DAS systems, a dropout mechanism with a probability p is also applied to the fitted trajectories. This effectively simulates the random missed detections, packet loss, and trajectory disconnections characteristic of actual DAS data, as illustrated in Fig. 8.

In addition to the similarity-based virtual detection, we can alternatively use DNN to recognize and delineate traffic trajectories. For instance, based on the authors' previous work (W. Zhang et al., 2025), the raw DAS signal matrix is mapped onto a two-dimensional image where the abscissa and ordinate represents the spatial channel index and temporal evolution, respectively. Formulating trajectory extraction as a pattern recognition task within these images, the trained DNN can segment the continuous high-intensity bands. This process recovers the spatiotemporal coordinates $\mathcal{T}_i = \{(x(t), t)\}$ for each vehicle i, and transforms raw optoelectronic modulation into discrete traffic trajectories.

To generate traffic flow and speed maps from microscopic trajectory data, the spatiotemporal trajectories on the t-s plane are partitioned into grid cells. The grid sizes along the t-axis and s-axis are Δ_t and Δ_s, respectively. For each cell, the traffic flow rate q is computed by dividing the cumulative vehicle displacement within the cell by the cell area. The space-mean speed v is then calculated as the ratio of Δ_s to the average travel time of all vehicles passing through that segment. In this way, the microscopic trajectory observations are aggregated into spatiotemporal maps of traffic flow and speed (Wang et al., 2024).

3.3. Traffic STM restoration

Data-driven deep learning models have achieved remarkable success in image restoration, when applied to DAS-based traffic state estimation, purely data-driven approaches face several important limitations. Data-driven approaches rely heavily on the assumption that the training data encompasses all possible state distributions. However, a DNN trained solely on minimizing the mean squared error (MSE) of available labels may yield predictions that are statistically plausible but physically unrealistic, such as negative densities, instantaneous velocity jumps, etc. In addition, the neural network models may struggle to generalize to unseen congestion patterns, such as stop-and-go waves, that are insufficiently represented in the training set.

Therefore, we construct a PINN framework. By embedding traffic flow differential equations directly into the loss function, we transform the learning problem from a supervised regression problem to a dual-objective optimization: fitting the observed sensor data while simultaneously satisfying the fundamental laws of traffic flow.

3.3.1 PINN models

To effectively map the coarse DAS-based STM to refined traffic state representations, we consider two different backbone architectures: the residual U-Net (ResUNet) and the Fourier neural operator (FNO), as shown in Fig. 9.

In real-world applications, the size and resolution of traffic maps may vary significantly across different scenarios. In this regard, although standard U-Net architectures perform well in image segmentation tasks, they may fail to capture the complex and multi-scale propagation of traffic shockwaves due to their fixed receptive fields.

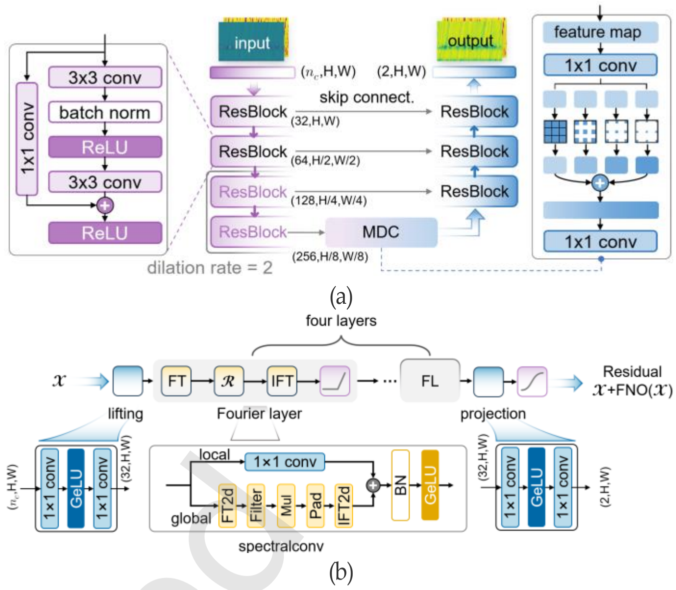

Fig. 9. Base models. (a) ResUNet; (b) FNO.

Therefore, we incorporate a multi-scale dilated convolution (MDC) module within the network's bottleneck. Traffic dynamics exhibit dependencies at various scales, ranging from local car-following behaviors to macroscopic congestion propagation spanning kilometers. Standard convolutions require deep stacking to enlarge the receptive field, which increases computational cost and risk of vanishing gradients. Dilated convolutions allow the network to expand its receptive field exponentially without reducing resolution or increasing the number of parameters. For instance, by fusing features from different dilation rates (e.g., 1,2,4,8 in Fig. 9(a)), the model simultaneously captures local interactions and long-range spatiotemporal dependencies. This design helps ensure that the reconstructed traffic jam upstream remains physically consistent with downstream flow conditions.

As a comparative baseline, we employ the FNO that approximates the solution operator of parametric partial differential equations (PDE). Unlike CNNs that operate in the local spatial domain, FNO performs global convolution in the frequency domain via Fast Fourier Transforms (FFT). A critical design choice in our FNO implementation is the use of the Gaussian error linear unit (GeLU) activation function instead of the standard ReLU. Physical constraints involve calculating high-order derivatives of the output (e.g.,$\partial q \,/\, \partial x$). ReLU introduces discontinuities in the first derivative at zero, which can destabilize the gradient descent process when optimizing PDE residuals. In comparison, GeLU provides a smooth, non-monotonic approximation, ensuring that the function is differentiable in each case, thereby facilitating stable backpropagation of the physical gradients.

To incorporate traffic flow laws into the training process, the hybrid loss function is defined as:

$$\mathcal{L}_{total} = \mathcal{L}_{data} + \lambda \mathcal{L}_{phy} \tag{6}$$

where $\mathcal{L}_{data}$ minimizes the reconstruction error against ground truth, $\mathcal{L}_{phy}$ varies based on the traffic flow theory applied, and λ denotes the weight of $\mathcal{L}_{phy}$.

In this study, we consider three levels of physical constraints: a) Lighthill-Whitham-Richards (LWR), b) LWR and fundamental diagram (FD), and c) Aw-Rascle-Zhang (ARZ)(Wang et al., 2026). We select LWR, LWR+FD, and ARZ in this study because they represent three commonly used traffic flow formulations with increasing levels of physical complexity. This comparison allows us to assess how different forms of physical prior influence learning performance in DAS-based TSP.

The LWR model assumes that traffic flow is conserved. Vehicles are neither created nor removed within the highway segment. The governing equation is the continuity equation as Eq. (7).

$$\frac{\partial q}{\partial x} + \frac{\partial \rho}{\partial t} = 0 \tag{7}$$

where q and ρ denote the traffic flow rate and density, respectively.

The corresponding residual loss $\mathcal{L}_{lwr}$ is computed using finite difference approximations for the partial derivatives as Eq. (8). To ensure numerical stability, the density is calculated with the predicted q and v as $\rho = q/(v+\epsilon)$. ϵ is 10^{-4} in this case.

$$\mathcal{L}_{lwr} = \frac{1}{n}\sum_{i}^{n} \left\| \frac{q(x+\Delta x) - q(x)}{\Delta x} + \frac{\rho(t+\Delta t) - \rho(t)}{\Delta t} \right\|^2 \tag{8}$$

The LWR model conserves mass but does not define the relationship between speed and density. To constrain the model to realistic equilibrium states, we introduce the Greenshields FD that assumes a linear relationship between speed and density, where V_f is free-flow speed and ρ_{jam} is jam density.

$$V_{eq}(\rho) = V_f\left(1 - \frac{\rho}{\rho_{jam}}\right) \tag{9}$$

In this case, the FD loss penalizes deviations of the predicted speed v from the theoretical equilibrium speed V_{eq} as Eqs. (10) to (11).

$$\mathcal{L}_{fd} = \frac{1}{n}\sum_{i}^{n} \left\| v_{pred} - \mathcal{C}\left(V_{eq}(\rho_{pred}), 0, V_f\right) \right\|^2 \tag{10}$$

$$\mathcal{C}(a,b,c) = \begin{cases} a, if\ a \in [b,c] \\ b, if\ a < b \\ c, if\ a > c \end{cases} \tag{11}$$

where v_{pred} and ρ_{pred} are predicted speed and density, respectively.

To capture non-equilibrium phenomena such as phantom traffic jams and hysteresis which LWR cannot model, we also consider the ARZ model that introduces a second equation for velocity evolution, treating speed as a dynamic variable rather than a static function of density, as Eq. (12).

$$\begin{cases} Conservation: \dfrac{\partial q}{\partial x} + \dfrac{\partial \rho}{\partial t} = 0 \\ Momentum: \dfrac{\partial (v + p(\rho))}{\partial t} + v\dfrac{\partial (v + p(\rho))}{\partial x} = \dfrac{V_{eq}(\rho) - v}{\tau} \end{cases} \tag{12}$$

where $p(\rho) = C_p \cdot \rho$ is the traffic pressure term representing drivers' anticipation of traffic conditions ahead, and τ is the relaxation time representing the delay in drivers adjusting their speed to the equilibrium velocity. $V_{eq}(\rho)$ is also estimated based on the Greenshields fundamental diagram.

The total physics loss of ARZ model combines the residuals of both the conservation and momentum equations.

$$\mathcal{L}_{arz} = \mathcal{L}_{mass} + \lambda_{mom}\mathcal{L}_{mom} \tag{13}$$

where

$$\mathcal{L}_{mom} = \frac{1}{n}\sum_{i}^{n} \left\| \frac{\partial (v + p(\rho))}{\partial t} + v\frac{\partial (v + p(\rho))}{\partial x} - \frac{V_{eq}(\rho) - v}{\tau} \right\|^2 \tag{14}$$

$$\mathcal{L}_{mass} = \mathcal{L}_{lwr} \tag{15}$$

Three levels of physical constraints are summarized in Tab. 2. As mentioned, this hierarchy of constraints allows us to evaluate how increasing physical complexity ranging from a first-order conservation law to a higher-order dynamic model assists the DNN models in restoring STM.

Table 2. Different constraints

Physical constraints	LWR	LWR+FD	ARZ
$\mathcal{L}_{phy}$	$\mathcal{L}_{lwr}$	$\mathcal{L}_{lwr} + \lambda_{fd}\mathcal{L}_{fd}$	$\mathcal{L}_{lwr} + \lambda_{mom}\mathcal{L}_{mom}$

3.3.2 Data fusion

In practical applications, data collected by camera or radars can be a complement to DAS. DAS systems offer the advantage of monitoring long-distance, continuous traffic flow dynamics, thereby providing a holistic view of the traffic dynamics on expressways. However, the conversion from raw optical vibration signals to macroscopic traffic parameters often suffers from signal noise and lower fidelity compared to visual observations. Conversely, video-based or radar sensors provide high-precision ground truth data but are spatially constrained, offering limited coverage only at specified locations. Therefore, we propose a heterogeneous data fusion framework that leverages the complementary characteristics of DAS and discrete surveillance cameras.

To construct a robust composite input for the TSP model, we implement a spatial substitution strategy within the STM. The base STM is initially derived from the continuous DAS signal, ensuring global spatiotemporal continuity. Subsequently, at spatial coordinates corresponding to camera deployment locations, the coarse DAS-derived flow and speed values are replaced by the accurate data extracted from the cameras. As such, we can obtain a hybrid input tensor where the majority of the domain is populated by DAS measurements, punctuated by islands of high-precision camera data, as illustrated in Fig. 10.

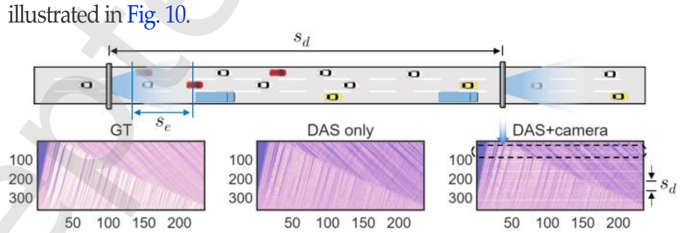

Fig. 10. Illustration of data fusion.

Let s_d and s_e be the spacing interval and the effective coverage range of cameras, respectively. In the experimental phase, we may treat s_d and s_e as adjustable hyperparameters and analyze their impact on the final accuracy of TSP as needed. This allows us to quantify the trade-off between infrastructure cost (density of cameras) and the marginal gain in prediction performance, thereby identifying the optimal integration for DAS-Camera cooperative sensing systems.

4 Validation of DAS Simulation

To empirically validate the effectiveness of the proposed DAS simulation framework, a synchronous data collection experiment was conducted. Real-world DAS signals and the corresponding roadside camera video footages were simultaneously recorded near the milepost K245+100 on the Chuxin Expressway in Fuyang, Anhui Province, as illustrated in Fig. 11. After the extraction of microscopic vehicle trajectories from the camera footages and their subsequent georectification into the road-aligned coordinate system, these empirical trajectories were fed into the DAS simulation procedure. This process can generate synthetic DAS acoustic signals, based on which the macroscopic spatiotemporal diagrams of traffic speed and flow were also derived.

Fig. 12(a) presents a side-by-side qualitative comparison between the simulated DAS acoustic signals and the field collected DAS data. Not surprisingly, the real-world DAS signals exhibit a more complex and heterogeneous noise profile. This discrepancy arises because the empirical data may be subjected to numerous unmodeled real-world variables, such as diverse vehicle axle weights, complex suspension dynamics, and unpredictable ambient environmental noises. For instance, if the fiber is not closely coupled to the expressway subgrade, the traffic-induced vibration may also be significantly weakened before being captured by the DAS system. Within the area highlighted by the solid box, the kinematic vehicle signatures in the real DAS data are almost entirely obscured by background noise, whereas they remain faintly observable in the simulated DAS map.

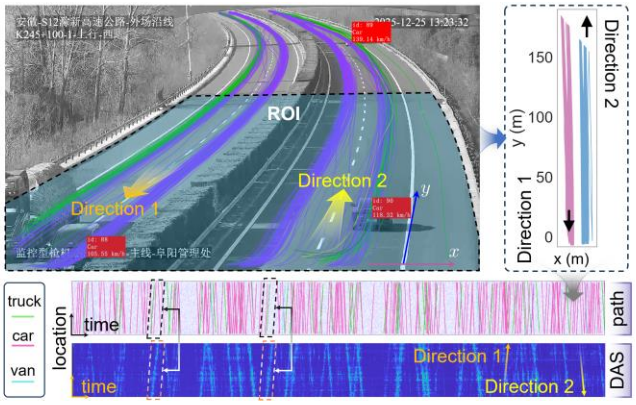

Fig. 11. Synchronous data collection on Chuxin Expressway.

Despite these localized differences in the signal-to-noise ratio, the simulated DAS spatiotemporal maps demonstrate a high degree of structural and macroscopic consistency with the ground truth. Notably, within the regions marked by dashed boxes, the morphological characteristics of the acoustic trajectory signatures (e.g., the slopes representing vehicle speeds and the intensity bands) exhibit similarity, indicating that the simulation effectively captures the fundamental vehicle-fiber interaction mechanics.

In addition, we evaluated the macroscopic traffic state outputs by comparing the spatiotemporal diagrams generated via the virtual detection module against those derived from actual DAS perception algorithms (W. Zhang et al., 2025), as shown in Fig. 12(b). Although minor discrepancies exist in the spatial distributions of absolute speed and flow values across the two travel directions, the statistical histograms show an overall alignment between the simulated and actual perception results.

This statistical and morphological consistency shown in Fig. 12 implies that the synthetic DAS data replicate the kinematic properties and inherent limitations (e.g., noise and missing data) of real-world optical fiber sensing. Therefore, it is viable to use the proposed DAS simulation framework as the testbed for the subsequent construction, training, and comparative evaluation of PINN models.

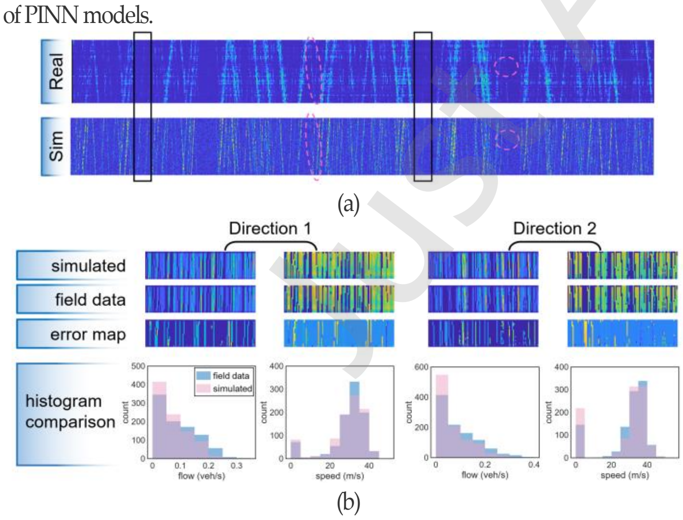

Fig. 12. Comparisons of field data and simulated results. (a) DAS signal; (b) flow and speed maps.

Note that while the simulation framework may capture the main traffic-induced spatiotemporal patterns expected in DAS observations and thus provide a realistic testbed for model development, transferring the proposed method to field deployment may require additional calibration, particularly with respect to sensor noise, fiber installation conditions, local vibration interference, and roadway-specific traffic characteristics. Although the learned physical structure is expected to generalize across sites, real DAS data may still be needed for fine-tuning the preprocessing pipeline and improving robustness under site-dependent conditions.

5 Experiment and Analysis

To evaluate the robustness and accuracy of the proposed PINN framework under diverse traffic conditions, we constructed a multi-scenario simulation pipeline. Considering that DNN model performance may vary significantly across different expressways and congestion levels, we first extracted seven distinct highway segment models using OpenStreetMap. Extensive microscopic traffic simulations were then conducted on these road networks with SUMO (Lopez et al., 2018), incorporating varying traffic volumes and vehicle class compositions. In this way, trajectory data of different scenarios were generated, enabling the application of subsequent DAS simulations. As illustrated in Fig. 13, the fundamental diagrams show that the simulated scenarios encompass a spectrum of traffic dynamics, ranging from sparse free-flow conditions to dense, congested stop-and-go waves.

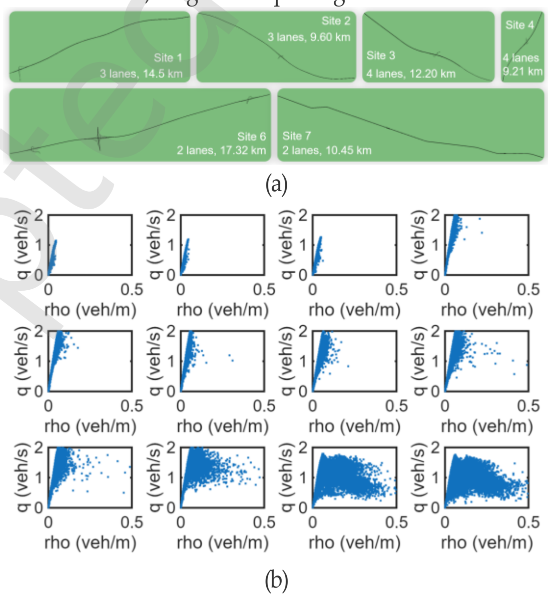

Fig. 13. Traffic Simulation. (a) 7 sites; (b) examples of fundamental diagrams.

Building upon the microscopic vehicle trajectories, we conducted the DAS simulation to generate both the GT traffic states and their corresponding DAS-based STM. The parameters controlling the DAS signal generation and noise injection are specified in Tab. 3. To construct a diverse training dataset for the PINN, these continuous STM were segmented into discrete patches using different spatial and temporal resolutions ($\Delta s \in [20,50]$, unit: s, and $\Delta t \in [10,40]$, unit: m). Finally, the data generation and segmentation process produced a dataset comprising 7,322 independent spatiotemporal samples. The dataset was further partitioned into training, validation, and testing sets with a 6:2:2 split ratio.

Table 3. Parameter values of DAS simulation

(a) Physic parameters of DAS

Modules	Parameter	Values
System configuration	Cable length L_e and simulation time	Vary with sites
	Gauge length L_g (m)	10
	Spatial resolution Δx (m)	1
	Sampling rate f_s(Hz)	400
Physics DAS model	Lateral distance from cable optic to the inner lane edge (m)	1.5
	Geometric decay index	1.0
	Material absorption	0.02
	Spatial spread σ_g(m)	15
	Wave velocity (m/s)	250

	Coupling efficiency η_c	1.0
	Background noise level	0.02
Noise parameters	Instrument noise level	0.02
	Coherent noise level	0.01
Virtual detection	Threshold IoU_t	0.3
	Dropout probability p	0.2

(b) Vehicle parameters for vibration signal generation

Vehicle types	Amplitude factor A_{base}	Frequency factor	Axle count N_{ax}
Small	1	1.2	2
Medium	2.5	1	2
Truck	5.0	0.7	5
Bus	4.0	0.8	2

5.1. Model comparisons

To analyze the impact of different network architectures, physical constraints, and data fusion strategies, we designed a comparative experimental matrix. The experiments consider combinations of two baseline architectures (i.e. ResUNet and FNO), three physical constraints (i.e. LWR, LWR+FD, and ARZ), and variations in input channel configurations. This combinatorial approach results in the development of 16 different PINN models. The weights of physical constraints are presented in Tab. 4 while traffic flow model parameters are specified in Tab. 5.

Note that when DAS-measurements are used as the third channel, raw DAS measurements are converted into a spatiotemporal image indexed by space and time before being used as model input. This representation is then normalized and resized to provide a unified input format for network training. The preprocessing is designed to retain the dominant traffic-related spatiotemporal patterns relevant to macroscopic state estimation, while reducing data dimensionality and suppressing local signal fluctuations.

As a result, the processed input may preserve mesoscopic traffic structures, such as congestion patterns and state transition fronts, but does not fully retain the complete fine-scale content of the original DAS signal. In particular, high-frequency details, localized disturbances, and native-resolution amplitude variations may be attenuated during compression and resizing.

Table 4. Weight of Physical Constraints

Type	λ_{lwr}	λ_{fd}	λ_{mom}
Weight	0.1	0.05	0.1

Table 5. Traffic constraints parameters

Constraints	Parameter	Value
LWR+FD	V_f (m/s)	39.48
	ρ_{jam}(veh/m)	0.15
ARZ	C_p(m^2/s)	50
	τ (s)	10

All 16 models were trained and tested on the same hardware (RAM of 32 GB, Intel®, GPU of GeForce RTX 4090). Furthermore, the training configurations were kept consistent across all models to avoid potential bias. Specifically, each model was trained for 100 epochs utilizing the Adam optimizer, with identical learning rate schedules and batch sizes (32 in this case). This controlled environment ensures that any performance discrepancies observed during the testing phase are attributable to the model architectures, input modalities, and the embedded physical laws, rather than computational or hyperparameter variances.

Table 6. Accuracy comparisons

(a) two channels

Models	Flow		Speed	
	RMSE	MAE	RMSE	MAE
res	0.036	0.028	1.381	1.092
res_lwr	0.025	0.018	1.205	0.939
res_fd	0.026	0.018	1.284	1.009
res_arz	0.060	0.042	2.229	1.784
fno	0.039	0.022	2.086	1.657
fno_lwr	0.039	0.021	2.108	1.687
fno_fd	0.056	0.040	2.207	1.774
fno_ud	0.433	0.403	5.679	4.933
fno_arz	0.066	0.045	2.807	2.280

(b) three channels

Models	Flow		Speed	
	RMSE	MAE	RMSE	MAE
res	0.040	0.032	1.405	1.116
res_lwr	0.026	0.017	1.308	1.026
res_fd	0.025	0.018	1.328	1.046
res_arz	0.095	0.063	4.465	3.608
fno	0.038	0.022	2.039	1.621
fno_lwr	0.038	0.022	2.006	1.592
fno_fd	0.054	0.040	2.150	1.730
fno_ud	0.488	0.479	5.226	4.544
fno_arz	0.107	0.070	4.783	3.877

By comparing the predictive performance of the 16 model variants on the test set, measured by root mean square error (RMSE) and mean absolute error (MAE), several insights regarding physical constraints, input configurations, and network architectures can be drawn as follows.

As noted in Tab. 6 and Fig. 14, across both the two-channel input (DAS-based flow and speed maps) and the three-channel input (incorporating the raw DAS signal) configurations, a consistent performance hierarchy emerges among the physical constraints. More specifically, DNN models constrained by the first-order LWR model achieve the highest accuracy, followed closely by those utilizing the LWR+FD constraints. Conversely, incorporating the second-order ARZ constraint severely degrades model performance, rendering it significantly inferior to the data-driven baseline (i.e. the unconstrained deep neural network). This degradation is even pronounced under the three-channel configuration. Similar finding have also been reported by existing studies (Lei et al., 2025).

The better performance of the LWR-constrained model suggests that, for DAS-based traffic state restoration, a simpler first-order physical prior may be more effective than more complex formulations. Since the DAS-derived representation mainly preserves coarse spatiotemporal traffic patterns, the conservation-based LWR constraint is sufficient to regularize the learning process. The ARZ model introduces complex momentum equations that require the computation of coupled and higher-order derivatives. However, DAS-based STM, even after processing, may inherently contain high-frequency noise. Computing higher-order physical residuals on noisy data amplifies this noise, leading to gradient explosions and destabilizing the training process. In addition, the strict calibration of ARZ parameters may not universally generalize across the highly heterogeneous traffic scenarios in our dataset, whereas the simpler mass conservation of the LWR model serves as a more robust regularizer.

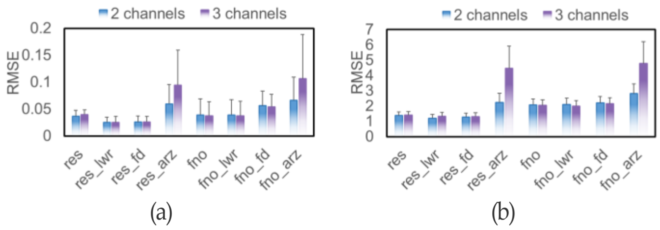

Fig. 14. Accuracy results. (a) flow; (b) speed.

Overall, transitioning from a two-channel to a three-channel input by injecting the raw DAS signal matrix may generally improve the prediction accuracy, as shown in Fig. 14. This result indicates that the raw optoelectronic data may contain latent kinematic signatures that are lost during conventional signal-to-traffic conversion. However, the degree of improvement is inconsistent across models. Notably, for the LWR-constrained models, the addition of the third channel paradoxically results in a decrease in accuracy.

This counterintuitive phenomenon is likely caused by spatial-temporal resolution mismatches. The raw DAS signal matrix possesses a much higher frequency and larger dimension than the macroscopic traffic state diagrams. To concatenate them as a unified input tensor, the raw DAS matrix must undergo arbitrary resizing and downsampling. This forced dimensional reduction may inevitably lead to the loss of critical microscopic vibration features and introduces interpolation artifacts. When the strict LWR mass conservation constraint is applied to these distorted and downsampled features, it creates a conflict between the data loss and the physics loss, and thereby affects the final prediction.

The comparative analysis of the backbone architectures reveals that while both the ResUNet and the FNO can effectively predict traffic STM, the ResUNet-based models consistently outperform the FNO models in overall accuracy, regardless of the input modalities. STMs, especially those containing congestion and stop-and-go waves, are characterized by sharp, localized discontinuities (the edges of shockwaves). The ResUNet that uses multi-scale dilated convolutions and skip connections, is designed to preserve these sharp spatial boundaries and pixel-level localized features. In contrast, the FNO models operate in the frequency domain, which prioritizes the learning of global, continuous, and low-frequency patterns. As a result, the FNO may tend to over-smooth the sharp transition zones between free-flow and congested states, leading to higher localized errors compared to the precise and localized feature extraction capabilities of the ResUNet.

Figs. 15(a) and 15(b) provide qualitative and quantitative evidence, respectively, of the model performance across different architectures and physical constraints. In Fig. 15(a), the top two rows compare the predicted STM of q and v against the GT. Overall, most models are able to reproduce the main traffic patterns, but clear differences can be observed in their ability to preserve local structures and intensity variations. The histogram comparisons in the third and fourth rows further illustrate the alignment between prediction and GT. A greater overlap between the two distributions indicates better statistical consistency. From this perspective, the ResUNet-based models, particularly res_lwr, show the closest match to the GT distributions, while the ARZ-constrained variants show more substantial deviations.

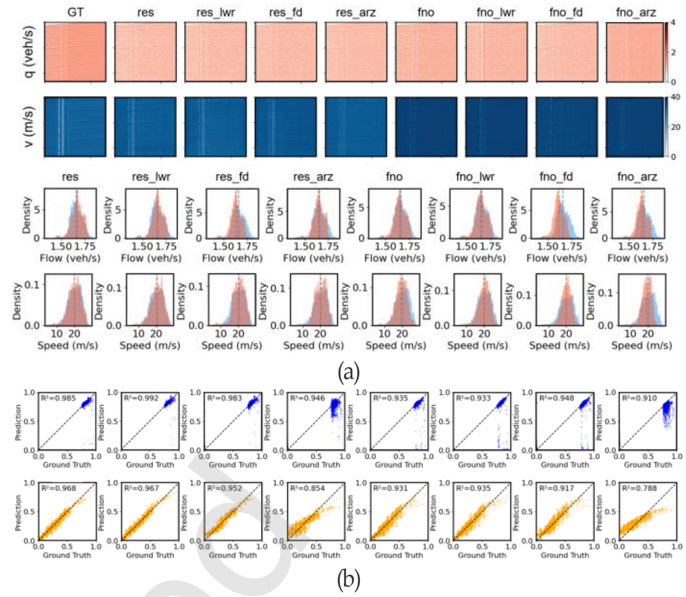

Fig. 15. Comparison of different models on a specific example (2 channels). (a) qualitative; (b) quantitative.

Fig. 15(b) quantitatively evaluates the correlation between the predictions and GT. In general, points clustering more tightly around the dashed line indicate higher accuracy and lower systematic bias. The corresponding R^2 values confirm the qualitative observations from Fig. 15(a). For flow estimation, res_lwr achieves the best performance ($R^2 = 0.992$), followed by res and res_fd, whereas the FNO-based models show relatively weaker agreement. A similar trend can be observed for speed estimation. The ResUNet family maintains consistently high accuracy, while the ARZ-based models, especially fno_arz, suffer the most severe degradation. Similar results can be drawn from Fig. 16, and these results are in accordance with Fig.14.

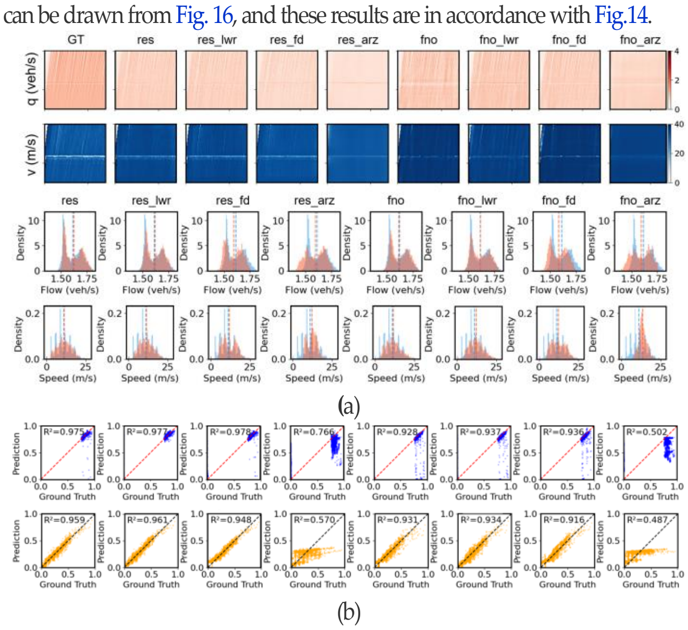

Fig. 16. Comparison of different models on a specific example (3 channels). (a) qualitative; (b) quantitative.

To gain a better understanding of the performance characteristics of the optimal model (res_lwr in this case), an error distribution analysis was conducted. Fig. 17 illustrates the relationship between the prediction error and the GT traffic flow rate, as well as the GT traffic speed. Overall, the magnitude of the prediction error exhibits a negative correlation with both the GT flow and speed, revealing specific operational boundaries of the model.

Regarding traffic flow, the error distribution displays a U-shaped trend.

At very low flow rates, the prediction error is relatively high. As the flow increases and approaches a critical intermediate value, the error gradually decreases, reaching a global minimum. However, as the flow continues to increase beyond this critical threshold toward road capacity, the error begins to increase again. Despite this secondary increase, the most significant deviations occur in the low-flow regime, as shown in Fig. 17(a).

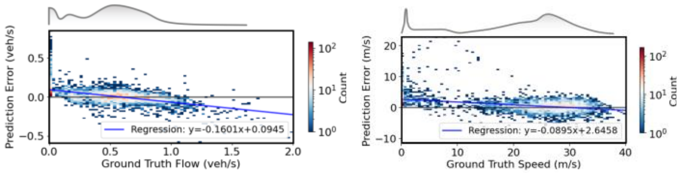

(a) (b)

Fig. 17. Relationship between prediction errors and traffic state. (a) flow; (b) speed.

This phenomenon in Fig. 17 can be attributed to the signal-to-noise ratio of the DAS system. At the critical flow state, the continuous stream of vehicles provides a strong, stable, and highly identifiable acoustic signature, optimizing the model's extraction capabilities. As traffic transitions into highly saturated states, the overlapping acoustic signatures of densely packed vehicles create signal interference, and thus degrade the DAS's capability of isolating individual vehicle impacts.

The speed error distribution reveals a negative correlation with the GT. In low-speed regimes, typically representing severe congestion or stop-and-go waves, the model exhibits substantial errors and demonstrates a bias towards overestimating the actual velocity. Conversely, during high-speed, free-flow conditions, the prediction error converges to a minimum, indicating highly reliable estimations.

This overestimation bias in congested states stems from both the DAS sensing mechanism and the inherent limitations of the LWR constraint. Physically, DAS systems are highly sensitive to dynamic strain. Vehicles moving at very slow speeds may generate significantly weaker dynamic signatures compared to fast-moving vehicles. As a result, the sensing system may neglect the nearly stationary vehicles, prompting the network to interpolate or spatially average the higher speeds of adjacent, moving vehicles. Mathematically, the first-order LWR physical constraint enforces conservation based on a macroscopic equilibrium assumption. It inherently tends to smooth out abrupt, localized velocity drops characteristic of severe congestion, thereby inflating the predicted speed in heavily congested temporal-spatial regions.

5.2. Influence of data fusion

To investigate the impact of camera deployment density on the accuracy of the PINN model, we separately reconstructed three datasets derived from the original training dataset, as illustrated in Fig. 18. Specifically, we considered three spatial intervals for camera placement: 1.0 km, 1.5 km, and 2.0 km, generating corresponding training datasets for each scenario. The res_lwr architecture that has demonstrated superior performance in the previous evaluations, was selected as the baseline model for this sensitivity analysis. The model was subsequently retrained from scratch on each new dataset. To ensure a fair comparison, all training configurations and hyperparameters were set identical to those employed in the initial model training phase.

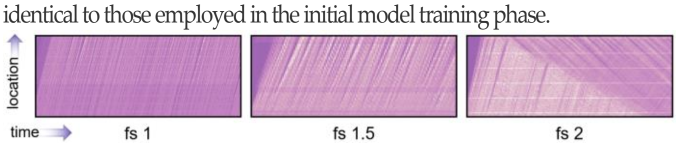

Fig. 18. Illustration of fused STM as input.

Based on results in Fig. 19, it is true that fusing DAS input with camera-captured data may overall help improve the accuracy of TSP. However, a smaller spacing of camera sensors does not guarantee a better model performance. The counterintuitive phenomenon where denser camera integration (1 km spacing) degrades model performance compared to sparser integration (2 km) can be primarily attributed to conflicts between the hard replacement data fusion strategy and the mathematical mechanisms of the physics-informed model.

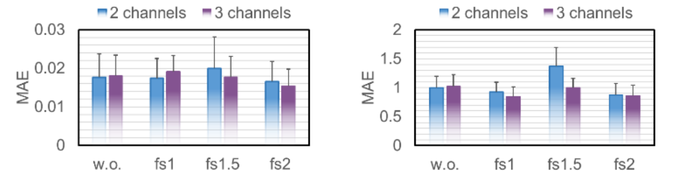

(a) (b)

Fig. 19. Accuracy performance of data fusion. (a) flow; (b) speed.

Directly substituting DAS estimations with precise camera ground truth may introduce high-frequency discontinuities, or spatial step changes, into the input matrix. Because the LWR constraint relies on computing spatial derivatives (i.e. $\partial q/\partial x$), these artificial boundaries cause the computed derivatives to spike exponentially at the sensor locations. This induces a gradient explosion within the physics loss function, which somehow destabilizes the network's convergence process. Consequently, a 1-km spacing doubles the frequency of these destabilizing mathematical anomalies compared to a 2 km interval. In addition, this rigid data insertion may conflict with the receptive field mechanism of the ResUNet architecture. Convolutional kernels are optimized to extract continuous, smooth macroscopic features, such as propagating traffic shockwaves. Imposing dense and accurate data 'stripes' may somehow disrupt these natural spatiotemporal textures.

To further improve the accuracy performance of PINN, a more sophisticated fusion strategy can be explored in the future.

5.3. Feasibility of Transfer Learning

In practical engineering applications, traffic dynamics on real-world expressways may exhibit substantial domain shifts compared to the scenarios covered by the simulated training data. To evaluate the transferability and environmental adaptability of the proposed PINN framework, we conducted a transfer learning experiment using the empirical NGSIM (Next Generation Simulation) trajectory dataset. The res_lwr, which has demonstrated better performance in previous evaluations, was again selected as the base pre-trained model for this experiment.

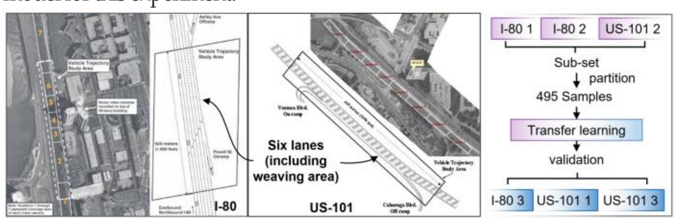

Fig. 20. Creation of transfer learning samples.

As shown in Fig. 20, we focused on the US-101 and I-80 highway segments in the NGSIM dataset. To construct the fine-tuning dataset, we separately extracted subset 2 from the US101 dataset and subsets 1 and 2 from the I-80 dataset. These empirical trajectory data were further processed under different spatiotemporal resolutions to generate a specialized small-scale transfer dataset containing 495 samples.

A key challenge in this experiment arises from the structural discrepancy between the source-domain simulation data and the target-domain NGSIM data. The original simulation dataset was generated on relatively simple highway segments with 2 to 4 lanes, whereas the NGSIM segments feature 6 lanes including complex weaving sections. Such geometric and operational complexity induces intricate lane-changing behaviors and turbulent traffic trajectory patterns, thereby creating a pronounced domain gap for the pre-trained model.

Fig. 21 shows the training loss curve during the transfer learning phase. The results show that, despite the increased complexity of the empirical traffic data, the model remains trainable and converges effectively during fine-tuning. Quantitatively, the prediction versus ground truth scatter plots (Fig. 22) demonstrate a substantial improvement in model accuracy. The correlation coefficient (R^2) for both flow and speed estimates increased significantly after transfer learning, indicating that the model successfully recalibrated its internal feature mappings to the new traffic patterns.

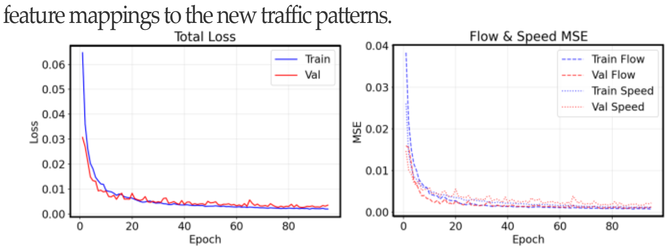

Fig. 21. Loss curve of transfer learning.

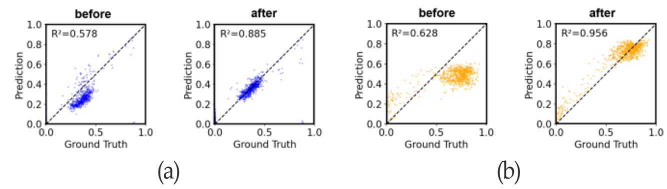

Fig. 22. prediction vs GT. (a) flow; (b) speed.

The effect of domain adaptation is even more clearly illustrated by the statistical histograms in Fig. 23. Before transfer learning, the zero-shot application of the pre-trained model resulted in a significant underestimation of traffic flow rates, with the predicted flow distribution diverging largely from the ground truth. However, after applying transfer learning, the predicted distributions of both traffic flow and speed become much more consistent with the empirical data, with substantial overlap observed between prediction and ground truth.

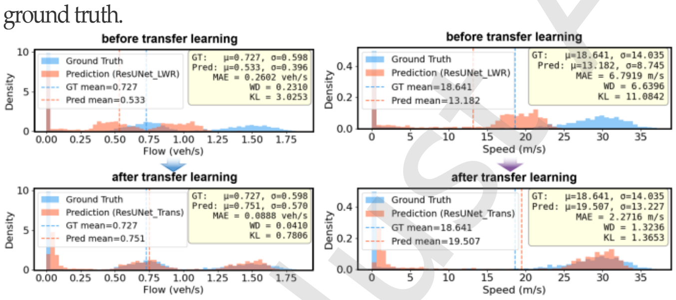

Fig. 23. Histograms of flow and speed.

To further examine the efficacy of the fine-tuning process, the transferred model was tested on the remaining NGSIM datasets including subsets 1 and 3 of US101, and subset 3 of I-80. As noted in Fig. 24, the model's ability to reconstruct spatiotemporal diagrams was substantially improved. Across the three test subsets, the fine-tuned model effectively recovered the detailed spatiotemporal textures of the traffic flow, as marked with dashed rectangles. The fine-tuned model successfully captured the macroscopic wave fluctuations, including the backward propagation of congestion shockwaves triggered by the complex weaving behaviors, which the original un-tuned model failed to resolve clearly.

These results imply potential of practical engineering application. Although a generalized physics-informed model may experience initial performance degradation when deployed in a highly divergent or structurally complex novel environment, its underlying physical representations remain robust. By utilizing a relatively small sample of scenario-specific empirical data (few-shot learning) to fine-tune the pre-trained network, its accuracy and reliability can be quickly restored and optimized. This strategy offers a highly cost-effective and scalable approach for deploying advanced TSP models across diverse real-world expressways.

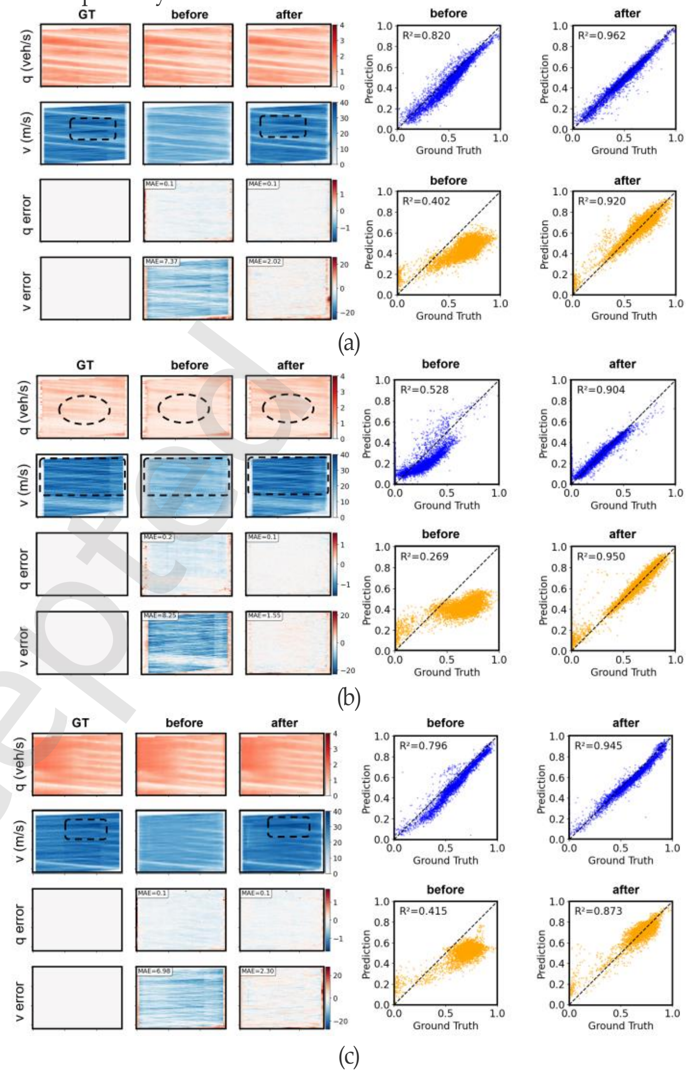

Fig. 24. Application of transfer learning. (a) I-80 3; (b) US-101 1; (c) US-101 3.

6 Concluding remarks

This study investigated the feasibility of using DAS data for large-scale traffic state perception on expressways. To our best knowledge, this study serves as the first attempt to explore long-distance TSP using DAS data. Based on the findings of this study, the following comments are offered.

- The proposed PINN framework can effectively improve the accuracy of the coarse STM derived from DAS. When properly developed, we may repurpose unused or spare fibers as a distributed traffic 'neural network', which enable the simultaneous addressing of scalability and operational feasibility.
- Among the tested physics constraints, the LWR model achieved the best overall performance, indicating that incorporating appropriate traffic flow physics can substantially enhance the quality of DAS-based TSP.
- Fusing DAS-derived STM with traffic observations collected from roadside cameras can further improve perception accuracy. However, the magnitude of improvement is closely related to the camera deployment configuration. This suggests that multimodal data fusion is a promising direction for improving large-scale traffic sensing, while the effectiveness of the fusion strategy is related to the spatial design of the sensing system.
- Few-shot transfer learning is effective in improving the accuracy of the

model when applied to new traffic environments. This finding is of clear practical significance, as it indicates that the proposed PINN framework can be adapted to specific deployment sites through fine-tuning with a limited amount of local data, thereby improving its applicability in real-world engineering scenarios.

Several issues remain to be addressed in future work. Currently, the model input mainly consists of a three-channel representation combining raw DAS data and coarse STM. However, the construction of the DAS image requires signal compression and spatial resizing, which inevitably causes information loss. Future studies should therefore consider a dual-branch network architecture to better preserve and extract features from raw DAS signals.

When investigating the fusion of camera data and DAS data, this study only considered the effect of camera spacing. Other important deployment factors, such as camera coverage range and field of view, should be further examined to better understand their influence on fusion performance. Also, the present study was conducted mainly within a simulation-based framework. Although the simulation procedure was carefully designed, future research should include a broader range of real-world scenarios to establish a benchmark dataset for DAS-based TSP. Such a benchmark would provide a more solid foundation for model evaluation, comparison, and practical deployment. Fiber installation quality is also an important factor that should be explicitly considered when extending the method to broader real-world applications in the future.

Appendix

A. DAS Simulation Demo

A video demo of DAS simulation is available online.

B. Transfer learning

Fig. B1 shows the heatmaps of the relationship between prediction error and ground-truth traffic speed before and after transfer learning. The heatmaps represent the local density of samples, while the zero-error line denotes the ideal case of unbiased prediction. Accordingly, the closer the fitted regression line is to the zero-error line, the higher the prediction accuracy of the model. It can be observed that, after transfer learning, the regression lines shift markedly toward the zero-error line in all three cases, suggesting a substantial reduction in prediction bias and error magnitude. These results confirm that transfer learning significantly enhances model performance in traffic speed estimation.

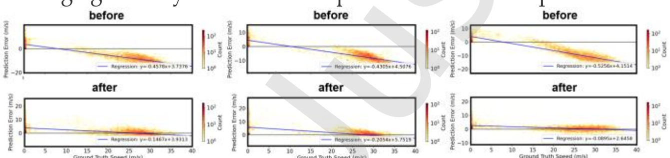

Fig. B1. Relationship between prediction error and ground-truth traffic speed.

Nomenclature

Acronym	Meaning
DAS	Distributed Acoustic Sensing
DNN	Deep Neural Network
FBG	Fiber Bragg Grating
FD	Fundamental Diagram
FFT	Fast Fourier Transforms
FNO	Fourier Neural Operator
GeLU	Gaussian error Linear Unit
GT	Ground Truth
MAE	Mean Absolute Error
MDC	Multi-scale Dilated Convolution
ML	Machine Learning
PDE	Partial Differential Equations
PIDL	Physics-Informed Deep Learning
PINN	Physics-Informed Neural Network
ResUNet	Residual U-Net
RMSE	Root Mean Square Error
STM	Spatiotemporal Traffic Map
TSP	Traffic State Perception

Author contributions

Yang Ma: Writing – original draft, Validation, Software, Methodology, Formal analysis, Data curation, Conceptualization. **Dianwei Zhou:** Writing – original draft, Software, Methodology, Formal analysis, Data curation. **Yang Liu**: Writing – review & editing, Software, Data curation, Funding acquisition. **Yu Kang:** Writing – review & editing, Supervision, Methodology, Funding acquisition. **Wenjun Lv:** Writing – review & editing, Formal Analysis, Methodology. **Said M. Easa:** Writing – review & editing, Formal analysis, Data curation. **Yiik Diew Wong:** Writing – review & editing, Formal Analysis, Methodology.

Replication and data sharing

The source codes and replication package are available on ETS data at https://doi.org/10.26599/ETSD.2026.9190030.

Acknowledgements

This work was jointly supported by the Regional Joint Funds of the National Natural Science Foundation of China [grant number: U25A20454], the National Natural Science Foundation of China [grant number: T2588101, 52402402], Anhui Provincial Natural Science Foundation [grant number: 2508085QE155], Fundamental Research Funds for the Central Universities [grant number: JZ2025HGTB0215], and the Natural Science Foundation in Anhui Province [grant number: 2408085J028].

Declaration of competing interest

The authors have no competing interests to declare that are relevant to the content of this article. The author Said M. Easa is the Editorial member of this journal.

Declaration of generative AI and AI-assisted technologies in the writing process

During the preparation of this work, the author(s) used Gemini 3.1 for minor language polishing. After utilizing this tool/service, the author(s) thoroughly reviewed and edited the content as necessary and take full responsibility for the final content of the published article.

References

Abewickrema, W., Yildirimoglu, M., Kim, J., 2026. A physics-informed deep learning framework for traffic state estimation in signalized arterial roads. *Transportation Research Part C: Emerging Technologies*, **182**, 105420.

Agrawal, S., Kanagaraj, V., Treiber, M., 2023. Two-dimensional LWR model for lane-free traffic. *Physica A: Statistical Mechanics and Its Applications*, **625**, 128990.

Almukhalfi, H., Noor, A., Noor, T. H., 2024. Traffic management approaches using machine learning and deep learning techniques: A survey. *Engineering Applications of Artificial Intelligence*, **133**, 108147.

An, Y., Ma, J., Xu, T., Cai, Y., Liu, H., Sun, Y., et al., 2023. Traffic vibration signal analysis of DAS fiber optic cables with different coupling based on an improved wavelet thresholding method. *Sensors*, **23**(12), 5727.

An, Z., Wu, Y., Zhang, F., Zhang, D., Gao, B., Zhang, S., et al., 2025. Long-term trajectory prediction method based on highway vehicle-following behavior patterns. *Journal of Intelligent and Connected Vehicles*, **8**(1), 9210045.

Antoniou, C., Koutsopoulos, H. N., Yannis, G., 2013. Dynamic data-driven local traffic state estimation and prediction. *Transportation Research Part C: Emerging Technologies*, **34**, 89–107.

Bi, J., Zhang, X., Yuan, H., Zhang, J., Zhou, M., 2022. A hybrid prediction method for realistic network traffic with temporal convolutional network and LSTM. *IEEE Transactions on Automation Science and Engineering*, **19**(3), 1869–1879.

Canudo, J., Sevillano, P., Preciado-Garbayo, J., Subías, J., Pastor, M. A., Ortega, A., et al., 2024. Smart traffic monitoring based on chirped-pulse distributed acoustic sensing. In: Optica Sensing Congress 2024 (AIS, LACSEA, Sensors, QSM), Paper SF5A.2.

Chen, Y., Wang, H., Min, R., Chen, Y., 2024. Recovering the invisible signals for urban traffic monitoring using distributed acoustic sensing. In: SEG/AAPG International Meeting for Applied Geoscience & Energy.

Chen, Z., Zhang, C.-C., Shi, B., Xie, T., Wei, G., Guo, J.-Y., 2024. Eavesdropping on wastewater pollution: Detecting discharge events from river outfalls via fiber-optic distributed acoustic sensing. *Water Research*, **250**, 121069.

Cohen, K., Hen, L., Lellouch, A., 2025. Training a distributed acoustic sensing traffic monitoring network with video inputs. *Scientific Reports*, **15**(1), 28954.

Darwish, A. M., Almansour, M., Salah, A., Zagow, M., Saeed, K., Elkafoury, A., 2024. Sensitivity evaluation of machine learning-based calibrated transportation mode choice models: A case study of Alexandria City, Egypt. *Transportation Research Interdisciplinary Perspectives*, **24**, 101052.

Deng, J., Jin, L., Wang, H., Zhang, Z., Liu, Y., Meng, F., et al., 2025. Distributed acoustic sensing for road traffic monitoring: Principles, signal processing, and emerging applications. *Infrastructures*, **10**(9), 228.

Di, X., Shi, R., Mo, Z., Fu, Y., 2023. Physics-informed deep learning for traffic state estimation: A survey and the outlook. *Algorithms*, **16**(6), 305.

Fakhruzi, I., Titos, M., Benítez, C., García, L., 2025. Urban traffic monitoring through distributed acoustic sensing: Trial analysis of a potent monitoring tool. *Measurement*, **253**, 117668.

Gao, H., Jia, H., Huang, Q., Wu, R., Tian, J., Wang, G., et al., 2024. A hybrid deep learning model for urban expressway lane-level mixed traffic flow prediction. *Engineering Applications of Artificial Intelligence*, **133**, 108242.

Guarda, P., Battifarano, M., Qian, S., 2024. Estimating network flow and travel behavior using day-to-day system-level data: A computational graph approach. *Transportation Research Part C: Emerging Technologies*, **158**, 104409.

Han, S., Huang, M.-F., Li, T., Fang, J., Jiang, Z., Wang, T., 2024. Deep learning-based intrusion detection and impulsive event classification for distributed acoustic sensing across telecom networks. *Journal of Lightwave Technology*, **42**(12), 4167–4176.

Hanson, D., 1972. On the product of the primes. *Canadian Mathematical Bulletin*, **15**(1), 33–37.

He, Y., An, C., Jia, Y., Liu, J., Lu, Z., Xia, J., 2024. Efficient and robust freeway traffic speed estimation under oblique grid using vehicle trajectory data. *IEEE Transactions on Intelligent Transportation Systems*, **25**(11), 16193–16206.

He, Z., Liu, Q., 2021. Optical fiber distributed acoustic sensors: A review. *Journal of Lightwave Technology*, **39**(12), 3671–3686.

Huang, A. J., Agarwal, S., 2020. Physics-informed deep learning for traffic state estimation. In: 2020 IEEE 23rd International Conference on Intelligent Transportation Systems (ITSC), 1–6. https://doi.org/10.1109/ITSC45102.2020.9294236

Huang, A. J., Agarwal, S., 2022. Physics-informed deep learning for traffic state estimation: Illustrations with LWR and CTM models. *IEEE Open Journal of Intelligent Transportation Systems*, **3**, 503–518. https://doi.org/10.1109/OJITS.2022.3182925

Huang, A. J., Agarwal, S., 2023. On the limitations of physics-informed deep learning: Illustrations using first-order hyperbolic conservation law-based traffic flow models. *IEEE Open Journal of Intelligent Transportation Systems*, **4**, 279–293. https://doi.org/10.1109/OJITS.2023.3268026

Hubbard, P. G., Ou, R., Xu, T., Luo, L., Nonaka, H., Karrenbach, M., et al., 2022. Road deformation monitoring and event detection using asphalt-embedded distributed acoustic sensing (DAS). *Structural Control and Health Monitoring*, **29**(11). https://doi.org/10.1002/stc.3067

Khacef, Y., Van Den Ende, M., Richard, C., Ferrari, A., Sladen, A., 2025. Precision traffic monitoring: Leveraging distributed acoustic sensing and deep neural networks. *IEEE Transactions on Intelligent Transportation Systems*, **26**(6), 7678–7689. https://doi.org/10.1109/TITS.2025.3556234

Khan, S. M., Dey, K. C., Chowdhury, M., 2017. Real-time traffic state estimation with connected vehicles. *IEEE Transactions on Intelligent Transportation Systems*, **18**(7), 1687–1699. https://doi.org/10.1109/TITS.2017.2658664

Kishida, K., Aung, T. L., Lin, R., 2024. Monitoring a railway bridge with distributed fiber optic sensing using specially installed fibers. *Sensors*, **25**(1), 98. https://doi.org/10.3390/s25010098

Klein, L. A., 2024. Roadside sensors for traffic management. *IEEE Intelligent Transportation Systems Magazine*, **16**(4), 21–44. https://doi.org/10.1109/MITS.2023.3346842

Lei, Y.-Z., Gong, Y., Chen, D., Cheng, Y., Yang, X. T., 2025. Potential failures of physics-informed machine learning in traffic flow modeling: Theoretical and experimental analysis. arXiv:2505.11491. https://doi.org/10.48550/arXiv.2505.11491

Li, M., Tang, J., Chen, Q., Liu, Y., 2023. Traffic arrival pattern estimation at urban intersection using license plate recognition data. *Physica A: Statistical Mechanics and Its Applications*, **625**, 128995. https://doi.org/10.1016/j.physa.2023.128995

Li, Y., Zhang, J., Yan, Y., Lau, A. P. T., 2026. Traffic monitoring using optical fiber distributed acoustic sensing for metropolitan environments. *Journal of Lightwave Technology*, **44**(3), 913–929. https://doi.org/10.1109/JLT.2025.3642924

Lienhart, W., Strasser, L., Dumitru, V., 2023. Distributed vibration monitoring of bridges with fiber optic sensing systems. In: Experimental Vibration Analysis for Civil Engineering Structures. Limongelli, M. P., Giordano, P. F., Quqa, S., Gentile, C., Cigada, A., Eds. Springer Nature Switzerland, 662-671. https://doi.org/10.1007/978-3-031-39117-0_67

Liu, J., Li, H., Noh, H. Y., Santi, P., Biondi, B., Ratti, C., 2025. Urban sensing using existing fiber-optic networks. *Nature Communications*, **16**(1), 3091. https://doi.org/10.1038/s41467-025-57997-y

Liu, S.-J., Lam, W. H. K., Lam Tam, M., Fu, H., Ho, H. W., Ma, W., 2024. Network-wide speed–flow estimation considering uncertain traffic conditions and sparse multi-type detectors: A KL divergence-based optimization approach. *Transportation Research Part C: Emerging Technologies*, **169**, 104858. https://doi.org/10.1016/j.trc.2024.104858

Lopez, P. A., Behrisch, M., Bieker-Walz, L., Erdmann, J., Flötteröd, Y.-P., Hilbrich, R., et al., 2018. Microscopic Traffic Simulation using SUMO. In: 2018 21st International Conference on Intelligent Transportation Systems (ITSC), 2575–2582. https://doi.org/10.1109/ITSC.2018.8569938

Luo, X., Yu, H., Yuan, H., Wang, Y., 2024. A model and data dual-driven approach to traffic state estimation on freeways. In: 2024 5th International Conference on Computer, Big Data and Artificial Intelligence (ICCBD+AI), 114–119. https://doi.org/10.1109/ICCBD-AI65562.2024.00027

Ma, C., Huang, X., Zhao, Y., Wang, T., Du, B., 2025. GRU-LSTM model based on the SSA for short-term traffic flow prediction. *Journal of Intelligent and Connected Vehicles*, **8**(1), 9210051-1-9210051–10. https://doi.org/10.26599/JICV.2024.9210051

Narisetty, C., Hino, T., Huang, M.-F., Ueda, R., Sakurai, H., Tanaka, A., et al., 2021. Overcoming challenges of distributed fiber-optic sensing for highway traffic monitoring. *Transportation Research Record: Journal of the Transportation Research Board*, **2675**(2), 233–242. https://doi.org/10.1177/0361198120960134

Narri, V., Alanwar, A., Mårtensson, J., Pettersson, H., Nordin, F., Johansson, K. H., 2025. Situational awareness using set-based estimation and vehicular communication: An occluded pedestrian-crossing scenario. *Communications in Transportation Research*, **5**, 100190. https://doi.org/10.1016/j.commtr.2025.100190

Nie, T., Qin, G., Wang, Y., Sun, J., 2023. Towards better traffic volume estimation: Jointly addressing the underdetermination and nonequilibrium problems with correlation-adaptive GNNs. *Transportation Research Part C: Emerging Technologies*, **157**, 104402. https://doi.org/10.1016/j.trc.2023.104402

Ouellet, S. M., Dettmer, J., Lato, M. J., Cole, S., Hutchinson, D. J., Karrenbach, M., et al., 2024. Previously hidden landslide processes revealed using distributed acoustic sensing with nanostrain-rate sensitivity. *Nature Communications*, **15**(1), 6239. https://doi.org/10.1038/s41467-024-50604-6

Rahman, M. A., Jamal, S., Taheri, H., 2024. Remote condition monitoring of rail tracks using distributed acoustic sensing (DAS): A deep CNN-LSTM-SW based model. *Green Energy and Intelligent Transportation*, **3**(5), 100178. https://doi.org/10.1016/j.geits.2024.100178

Rempe, F., Loder, A., Bogenberger, K., 2021. Estimating motorway traffic states with data fusion and physics-informed deep learning. In: 2021 IEEE International Intelligent Transportation Systems Conference (ITSC), 2208–2214. https://doi.org/10.1109/ITSC48978.2021.9565096

Rossi, M., Wisén, R., Vignoli, G., Coni, M., 2022. Assessment of distributed acoustic sensing (DAS) performance for geotechnical applications. *Engineering Geology*, **306**, 106729. https://doi.org/10.1016/j.enggeo.2022.106729

Seo, T., Bayen, A. M., Kusakabe, T., Asakura, Y., 2017. Traffic state estimation on highway: A comprehensive survey. *Annual Reviews in Control*, **43**, 128–151. https://doi.org/10.1016/j.arcontrol.2017.03.005

Shi, R., Mo, Z., Di, X., 2021. Physics-informed deep learning for traffic state estimation: A hybrid paradigm informed by second-order traffic models. *Proceedings of the AAAI Conference on Artificial Intelligence*, **35**(1), 540–547. https://doi.org/10.1609/aaai.v35i1.16132

Song, A., Liu, A., Li, Z., Liu, G., Guo, A., Jiang, J., 2026. Triple-duty distributed acoustic sensing in urban environments: Concurrent subsurface imaging, pipeline diagnostics, and traffic surveillance. *Journal of Applied Geophysics*, **246**, 106117. https://doi.org/10.1016/j.jappgeo.2026.106117

Thomas, P. J., Heggelund, Y., Klepsvik, I., Cook, J., Kolltveit, E., Vaa, T., 2024. The performance of distributed acoustic sensing for tracking the movement of road vehicles. *IEEE Transactions on Intelligent Transportation Systems*, **25**(6), 4933–4946. https://doi.org/10.1109/TITS.2023.3339509

Tomasov, A., Zaviska, P., Dejdar, P., Klicnik, O., Da Ros, F., Horvath, T., et al., 2025. Advancing perimeter security: integrating DAS and CNN for object classification in fiber vicinity. *IEEE Access*, **13**, 63600–63610. https://doi.org/10.1109/ACCESS.2025.3558594

Trinh, X.-S., Keyvan-Ekbatani, M., Ngoduy, D., Robertson, B., 2024. Stochastic switching mode model based filters for urban arterial traffic estimation from multi-source data. *Transportation Research Part C: Emerging Technologies*, **164**, 104664. https://doi.org/10.1016/j.trc.2024.104664

Tu, C., Wang, L., Lim, J., Kim, I., 2024. Advancements and prospects in multisensor fusion for autonomous driving. *Journal of Intelligent and Connected Vehicles*, **7**(4), 245–247. https://doi.org/10.26599/JICV.2023.9210042

Urquijo, I. R., García, A. C., Cobo, L. R., Quintela Incera, M. Á., 2023. Real options of distributed DAS sensing applied to road transport engineering. *Transportation Research Procedia*, **71**, 323–330. https://doi.org/10.1016/j.trpro.2023.11.091

Wang, N., Wang, X., Yan, H., He, Z., 2024. From rectangle to parallelogram: An area-weighted method to make time-space diagrams incorporate traffic waves. *Digital Transportation and Safety*, **3**(1), 1–7. https://doi.org/10.48130/dts-0024-0001

Wang, T., Li, Y., Cheng, R., Zou, G., Dantsuji, T., Ngoduy, D., 2026. Knowledge-data fusion oriented traffic state estimation: A stochastic physics-informed deep learning approach. *Transportation Research Part C: Emerging Technologies*, **182**, 105422. https://doi.org/10.1016/j.trc.2025.105422

Wang, Y., Chen, Y., Zheng, L., 2025. Digital twin intersection based on roadside multi-sensor data fusion. *Digital Transportation and Safety*, **4**(4), 242–250. https://doi.org/10.48130/dts-0025-0023

Wang, Y., Papageorgiou, M., 2005. Real-time freeway traffic state estimation based on extended Kalman filter: A general approach. *Transportation Research Part B: Methodological*, **39**(2), 141–167. https://doi.org/10.1016/j.trb.2004.03.003

Wang, Y., Papageorgiou, M., Messmer, A., Coppola, P., Tzimitsi, A., Nuzzolo, A., 2009. An adaptive freeway traffic state estimator. *Automatica*, **45**(1), 10–24. https://doi.org/10.1016/j.automatica.2008.05.019

Wang, Z., Lu, B., Ye, Q., Cai, H., 2020. Recent Progress in Distributed Fiber Acoustic Sensing with Φ-OTDR. *Sensors*, **20**(22), 6594. https://doi.org/10.3390/s20226594

Xia, Z., Zhang, Y., Yang, J., Xie, L., 2024. Dynamic spatial–temporal graph convolutional recurrent networks for traffic flow forecasting. *Expert Systems with Applications*, **240**, 122381. https://doi.org/10.1016/j.eswa.2023.122381

Xie, T., Zhang, C.-C., Shi, B., Wang, Z., Zhang, S.-S., Yin, J., 2023. Seismic monitoring of rockfalls using distributed acoustic sensing. *Engineering Geology*, **325**, 107285. https://doi.org/10.1016/j.enggeo.2023.107285

Xu, D., Wei, C., Peng, P., Xuan, Q., Guo, H., 2020. GE-GAN: A novel deep learning framework for road traffic state estimation. *Transportation Research Part C: Emerging Technologies*, **117**, 102635. https://doi.org/10.1016/j.trc.2020.102635

Yuan, S., Lellouch, A., Clapp, R. G., Biondi, B., 2020. Near-surface characterization using a roadside distributed acoustic sensing array. *The Leading Edge*, **39**(9), 646–653. https://doi.org/10.1190/tle39090646.1

Zhang, G., Song, Z., Osotuyi, A. G., Lin, R., Chi, B., 2022. Railway traffic monitoring with trackside fiber-optic cable by distributed acoustic sensing Technology. *Frontiers in Earth Science*, **10**, 990837. https://doi.org/10.3389/feart.2022.990837

Zhang, J., Mao, S., Yang, L., Ma, W., Li, S., Gao, Z., 2024. Physics-informed deep learning for traffic state estimation based on the traffic flow model and computational graph method. *Information Fusion*, **101**, 101971. https://doi.org/10.1016/j.inffus.2023.101971

Zhang, K., Zhou, F., Wu, L., Xie, N., He, Z., 2024. Semantic understanding and prompt engineering for large-scale traffic data imputation. *Information Fusion*, **102**, 102038. https://doi.org/10.1016/j.inffus.2023.102038

Zhang, S. , Zhang, J. , Yang, L. , Chen, F. , Li, S. , Gao, Z., 2024. Physics guided deep learning-based model for short-term origin–destination demand prediction in urban rail transit systems under pandemic. *Engineering*, **41**(c), 276-296.

Zhang, Q., Zhou, L., Su, Y., Xia, H., Xu, B., 2023. Gated recurrent unit embedded with dual spatial convolution for long-term traffic flow prediction. *ISPRS International Journal of Geo-Information*, **12**(9), 366. https://doi.org/10.3390/ijgi12090366

Zhang, W., Li, C., Qi, Z., Xia, Q., Li, K., Kang, Y., et al., 2025. Expressway traffic trajectory recognition on DAS vibration spatiotemporal images. *IEEE Transactions on Intelligent Transportation Systems*, **26**(4), 5120–5134. https://doi.org/10.1109/TITS.2025.3540540

Zhang, Z., Yuan, Y., Li, M., Lu, P., Yang, X. T., 2025. Empirical study of the effects of physics-guided machine learning on freeway traffic flow modelling: Model comparisons using field data. *Transportmetrica A: Transport Science*, **21**(2), 2264949. https://doi.org/10.1080/23249935.2023.2264949

Zhao, M., Yu, H., Wang, Y., Song, B., Xu, L., Zhu, D., 2024. Real-time freeway traffic state estimation for inhomogeneous traffic flow. *Physica A: Statistical Mechanics and Its Applications*, **639**, 129633. https://doi.org/10.1016/j.physa.2024.129633

Zhou, X., Wu, Z., 2024. Research progress of pipeline health monitoring based on distributed fiber optic sensing. In: 2024 9th International Conference on Electronic Technology and Information Science (ICETIS), 273–280. https://doi.org/10.1109/ICETIS61828.2024.10593770

Zhu, H.-H., Liu, W., Wang, T., Su, J.-W., Shi, B., 2022. Distributed acoustic sensing for monitoring linear infrastructures: Current Status and Trends. *Sensors*, **22**(19), 7550. https://doi.org/10.3390/s22197550

Author biography

Yang Ma received the M.S. and Ph.D. degrees from the School of Transportation, Southeast University, Nanjing, China, in 2017 and 2022, respectively. He is currently an Associate Professor with the School of Automotive and Transportation Engineering, Hefei University of Technology. His research interests include infrastructure digitalization, cooperative vehicle-infrastructure systems, point cloud data processing, and road safety analysis.

Dianwei Zhou received the bachelor degree in transportation Engineering from Nantong University, Nantong, China, in 2025. He is currently a master student with the Hefei University of Technology. His research interests include ubiquitous traffic sensing and intelligent transportation systems.

Yang Liu received the Ph.D. degree from Southeast University, Nanjing, China, in 2021. Currently, he is an Associate Research Professor at the School of Vehicle and Mobility, Tsinghua University, China. His research interests include intelligent transportation systems, artificial intelligence techniques, and data mining, with applications in complex real-world problems, such as autonomous vehicles and urban mobility.

Yu Kang received the Ph.D. degree in control theory and control engineering from the University of Science and Technology of China (USTC), Hefei, China, in 2005. From 2005 to 2007, he was a Post-Doctoral Fellow with the Academy of Mathematics and Systems Science, Chinese Academy of Sciences, Beijing, China. He is currently a Professor with the Department of Automation, USTC, and Hefei University of Technology. His current research interests include artificial intelligence and atmospheric sciences.

Wenjun Lv received the Ph.D. degree in control science and engineering from the University of Science and Technology of China (USTC), Hefei, China, in 2018. He is currently an Associate Professor with the Department of Automation, USTC. His current research interests include interpretable machine learning and its applications in the energy industry.

Said M. Easa received the Ph.D. degree in transportation engineering from the University of California at Berkeley, Berkeley, CA, USA, in 1982. He is currently a Professor with the Department of Civil Engineering, Toronto Metropolitan University, Toronto, ON, Canada. He is a fellow of the Engineering Institute of Canada, the Canadian Academy of Engineering, and the Canadian Society for Civil Engineering (CSCE).

Yiik Diew Wong received the B.E. degree in civil engineering and the Ph.D. degree in transportation engineering from the University of Canterbury, New Zealand, in 1983 and 1990, respectively. He is currently an Associate Chair (Academic) and an Associate Professor with the School of Civil and Environmental Engineering, Nanyang Technological University (NTU), Singapore. His research interests include sustainable urban mobility, road safety engineering, driver behaviors, and active mobility.